Electronic Supplementary Material (ESI) for Dalton Transactions.

Supporting Information

Linker Permethylation as a Means to Foster Valence Tautomerism and Thwart Dimerization in Ferrocenyl-Triarylmethylium Cations

Moritz Nau,[a] Larissa A. Casper,[a] Gernot Haug,[a] Michael Linseis[a], Serhiy Demeshko[b] and Rainer F. Winter[a]*

[a] *Fachbereich Chemie, Universität Konstanz, Universitätsstraße 10, 78457 Konstanz (Germany); E-mail: rainer.winter@uni-konstanz.de.*
[b] *Institut für Anorganische Chemie, Georg-August-Universität Göttingen, Tammanstraße 4, 37077 Göttingen (Germany)*

General Methods. All syntheses and sample preparations were performed under an atmosphere of purified nitrogen with dry, distilled, and degassed solvents with standard Schlenk and glovebox techniques. Commercially available starting materials were used as purchased. Thioxanthone was prepared according to the literature procedure.[1] NBu_4^+ $[B\{C_6H_3(CF_3)_2\text{-}3,5\}_4]^-$ was used as supporting electrolyte in all electrochemical measurements and was synthesized according to an established two-step procedure starting from 3,5-bis(trifluoromethyl)bromobenzene to first give Na^+ $[B\{C_6H_3(CF_3)_2\text{-}3,5\}_4]^-$,[2] which was subsequently subjected to a cation exchange reaction.[3] BROOKHART'S acid was synthesized following a published protocol,[4] and was used for the conversion of the carbinol precursor into the corresponding cation.

NMR spectroscopy. ^{1}H-NMR (400 MHz), ^{19}F-NMR (376 MHz), and ^{13}C-NMR (101 MHz) spectra were recorded on a Bruker Avance III 400 spectrometer in the solvent indicated at room temperature (if not stated otherwise). The spectra were referenced to the residual protonated solvent (^{1}H) or the solvent signal (^{13}C). ^{19}F-NMR spectra were referenced to the external reference of the spectrometer ($\delta(^{19}F)$ = 0 ppm for $CFCl_3$).

ESI mass spectrometry. Mass spectra were recorded on a LTQ Orbitrap Velos (Thermo Scientific) with ESI capable of a resolution of at least 60000 in CH_2Cl_2 as a solvent. The spectrometer was calibrated with the Pierce LTQ Velos ESI Positive Calibration Solution (Thermo Fisher Scientific) prior to every measurement. Detection was done in the positive-ion mode. The observed data were compared to respective simulations of the molecules' MS patterns.

Elemental analysis. A C, H, N-analyzer (model Elementar vario MICRO Cube) by *Heraeus* was used for combustion analyses.

Cyclic voltammetry. Cyclic voltammetry was performed under an atmosphere of argon. The voltammograms were recorded using a BASi Epsilon potentiostat and a cell with a platinum electrode (Ø = 1.1 mm, BASi). The platinum electrode was polished before each measurement with diamond pastes with particle sizes of 1 µm and 0.25 µm from *Buehler & Witz*. An AgCl and a spiral-shaped Pt wire was used as the reference and counter electrode. NBu_4^+ $[B\{C_6H_3(CF_3)_2\text{-}3,5\}_4]^-$ was used in a concentration of 0.1 mM in CH_2Cl_2 as a supporting electrolyte. The redox potentials were calculated *versus* the FcH/FcH^+ redox couple.

EPR spectroscopy. Electron paramagnetic resonance (EPR) studies were conducted on a *X*-band spectrometer MiniScope MS5000 by Magnettech GmbH with the program ESR Studio 1.63.0.[5] A liquid nitrogen cooled thermostat was used in combination with the temperature controller HO3. EPR samples in dichloromethane were prepared and sealed inside a glovebox. All experiments were performed with identical measurement parameters: *B* = 330 mT-345 mT, Sweep Time = 60 s, modulation = 0.3 mT, power = 6.3096 mW. The spin counting method for the determination of the amount of diradical valence tautomer and dimerization was applied according to the literature.[6] Simulation of the measured EPR spectra was performed using the *Matlab* Easyspin program '*garlic*'.[7]

X-band EPR spectra at 10 K (samples in dichloromethane) were recorded on an ELEXSYS E580 spectrometer equipped with a super-high-Q probe head (both from *Bruker BioSpin*). Temperature control was realized with an ESR900 cryostat in combination with an intelligent temperature controller ITC503 (both from *Oxford Instruments*) with liquid helium used as a cooling agent. Experimental settings were adjusted to avoid any overmodulation and saturation effects:[8] Microwave frequency of 9.4 GHz, microwave attenuation of 36 dB, modulation ampli-

tude of 3 G, sweep width of 6000 G, and number of points of 8192. Data were baseline-corrected by subtracting a first-order polynomial. A background signal originating from the solvent was used for further corrections.[1]

Mößbauer spectroscopy. Samples used for Mößbauer spectroscopy were freshly prepared under inert gas atmosphere. A *WissEl* Mößbauer spectrometer with a ^{57}Co source in a Rh matrix, an alternating constant acceleration, and a *Janis* closed-cycle helium cryostat were operated in the transmission mode to record the spectra. Simulation of the recorded data was done with the *Mfit* program using *Lorentzian* line doublets.[9] The isomer shifts are given relative to iron metal at ambient temperature.[1]

X-ray diffraction analysis. X-ray diffraction analysis was performed using an STOE IPDS-II diffractometer equipped with a graphite-monochromated Mo-K_α radiation source (λ_{Mo} = 0.71073 Å). For detection, an image plate system at T = 100.15 K was used. The X-Area software package was used for data processing. Structures were solved using OLEX[10] with the ShelXT[11] structure solution program using intrinsic phase position. A semiempirical absorption correction was performed and the structure was solved by the heavy-atom method. Refinement was achieved with the ShelXL[12] package. All non-hydrogen atoms were refined with anisotropic displacement parameters, and hydrogen atoms were introduced in a riding model.[13] Crystallographic data were deposited at the Cambridge Crystallographic Data Centre and are available under deposition number CCDC 2240663.

Quantum chemical calculations. Quantum chemical calculations based on density functional theory (DFT) employed the Gaussian 16 program package.[14] Geometry optimization was followed by vibrational analysis. All calculations were performed in 1,2-dichloroethane as the solvent applying the polarizable continuum model (PCM).[15] Electronic spectra were calculated at the optimized ground-state structures by the time-dependent-DFT method. A Wachter basis set[16] was used for the Fe atom, and a 6-316(d)[17] polarized double-ξ basis set with PBE0[18,19] as correlation and exchange functional was used for the remaining atoms. The GaussSum,[20] Avogadro, GNU Parallel and vmd program packages were used in combination with POV-Ray for data processing,[21] and graphical representations.[21,22]

Absorption spectroscopy. All UV/Vis/NIR spectra were acquired with a TIDAS fiber optic diode array spectrometer, which consists of a combination of MCS UV/Vis and PGS NIR instruments from *j&m Analytic AG*. For the determination of the extinction coefficients, quartz cells with an optical path length of 0.1 cm, 0.5 cm, or 1 cm were used, which were purchased from *Hellma Analytics*.

Synthetic route forthe BAr^{F24-} salt of $FcDurSXanth^{CF3}$.

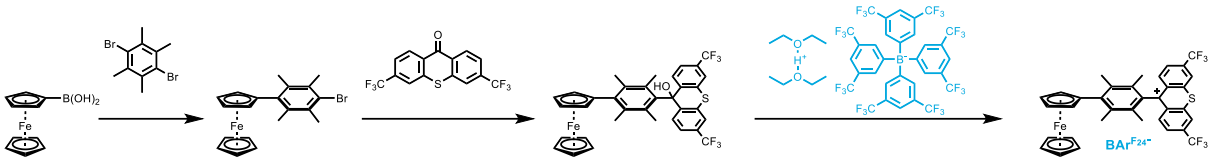

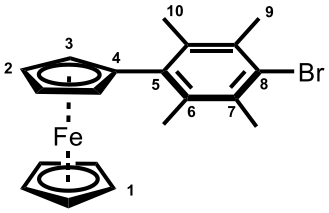

4-Ferrocenyl-(2,3,5,6-tetramethyl)bromobenzene

Ferrocene boronic acid (305.70 mg, 1.33 mmol, 1.00 eq.), 3,6-dibromodurene (388.38 mg, 1.33 mmol, 1.00 eq.) and $Pd(dppf)Cl_2$ (9.73 mg, 13.30 µmol, 0.01 eq.) were dissolved in degassed dimethyl glycol (15 mL). 2 M aqueous NaOH (239.98 mg, 2 mL, 6.00 mmol, 4.51 eq.) was added and the resulting solution was heated to 80° C for two days in a high-pressure reaction tube (suitable up to 12 bar). After quenching with water, the solution was extracted with CH_2Cl_2 and the combined organic phases were dried over Na_2SO_4. The crude product was purified by column chromatography on silica (*n*-pentane/ethyl acetate 1:0 - 1:4) to obtain 142 mg (0.36 mmol) of 4-ferrocenyl-(2,3,5,6-tetramethyl)-phenyl bromide as an orange solid in 27% yield.

^{1}H-NMR (CD_2Cl_2, 400 MHz) δ [ppm] = 4.37 (vt, $^3J_{HH}$ = 1.6 Hz, 2H, H-2/3), 4.23 (vt, $^3J_{HH}$ = 1.6 Hz, 2H, H-2/3), 4.17 (s, 5H, H-1), 2.54 (s, 6H, H-9/10), 2.46 (s, 6H, H-9/10).

^{13}C{^{1}H}-NMR (CD_2Cl_2, 101 MHz) δ [ppm] = 135.3 (C-6/7), 134.3 (C-6/7), 128.1 (C-8), 87.8 (C-5), 87.5 (C-4), 72.4 (C-2/3), 69.7 (C-1), 67.1 (C-2/3), 21.7 (C-9/10), 20.8 (C-9/10).

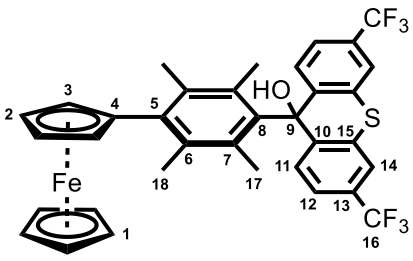

4-Ferrocenyl-(2,6-dimethyl)-phenyl-3,6-(di-trifluoromethyl)-10-thioxanthyl methyl alcohol (FcDurSXanth^{CF3}-OH)

4-Ferrocenyl-(2,3,5,6-tetramethyl)bromobenzene (40 mg, 0.10 mmol, 1.00 eq.) was dissolved in dry, degassed THF (2 mL). The solution was cooled to -78 °C and ^{t}BuLi (1.9 M in hexane, 12.90 mg, 0.11 mL, 0.20 mmol, 2.00 eq.) was added dropwise. The solution was stirred for one hour at -78 °C and subsequently without cooling for further 30 minutes and the cooled again to -78 °C. 3,6-Bis(trifluoromethyl)-9*H*-thioxanthen-9-one (35.08 mg, 0.10 mmol, 1.00 eq.) was prepared according to a published procedure,[1] dissolved in dry, degassed THF (2 mL), and added dropwise to the reaction mixture at -78 °C. A color change to brown was observed. The resulting mixture was stirred for one hour at -78 °C and then allowed to warm to room temperature and stirred overnight. Subsequently, the solution was heated to reflux for five hours. Then, the reaction was quenched by the addition of water (5 mL). Et_2O was added, the phases were separated and the aqueous phase was further extracted with Et_2O (3×50 mL). The combined organic phases were dried over Na_2SO_4 and the solvent was removed *in vacuo*. The crude product was purified by column chromatography on silica (PE/EE 1:0-93:7) and dried *in vacuo*. 18.20 mg (27.31 µmol) of target compound **FcDurSXanth^{CF3}-OH** were obtained as an orange solid in 27% yield.

^{1}H-NMR (CD_2Cl_2, 400 MHz) δ [ppm] = 7.72 (d, $^{4}J_{FH}$ = 0.7 Hz, 2H, H-14), 7.38 (dd, $^{3}J_{HH}$ = 8.3 Hz, $^{4}J_{FH}$ = 1.1 Hz, 2H, H-12), 7.29 (d, $^{3}J_{HH}$ = 8.4 Hz, 2H, H-11), 4.42 (vt, $^{3}J_{HH}$ = 1.8 Hz, 2H, H-3), 4.31 (vt, $^{3}J_{HH}$ = 1.8 Hz, 2H, H-2), 4.20 (s, 5H, H-1), 2.92 – 2.11 (m, 13H, H-17/18+OH).

^{13}C{^{1}H}-NMR (CD_2Cl_2, 101 MHz) δ [ppm] = 142.9 (C-13), 138.3 (C-9), 136.1 (C-8), 135.9 (C-5), 130.6 (C-15), 130.2 (C-7), 130.0 (C-6), 129.9 (C-11), 123.9 (d, $^{1}J_{CF}$ = 273 Hz, C-16), 123.6 (q, $^{3}J_{CF}$ = 3.5 Hz, C-12), 123.3 (q, $^{3}J_{CF}$ = 3.9 Hz, C-14), 88.4 (C-4), 80.6 (C-5), 72.8 (C-2), 70.0 (C-1), 67.5 (C-3), 15.5 (C-18), 14.4 (C-17).

^{19}F{^{1}H}-NMR (CD_2Cl_2, 376 MHz) δ [ppm] = -62.1 (s, -CF_3-16).

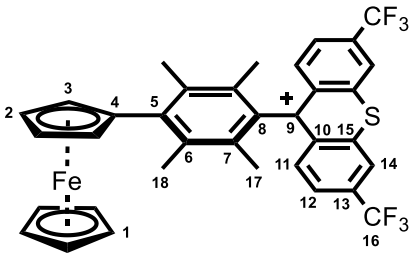

4-Ferrocenyl-(2,3,5,6-tetramethyl)-phenyl-3,6-(di-trifluoromethyl)-10-thioxanthyl methylium (**FcDurSXanth^{CF_3}**)

The carbinol precursor **FcDurSXanth^{CF_3}-OH** was dissolved in dry, degassed CH_2Cl_2 and was treated with exactly 1 eq. of BROOKHART's acid, which was prepared to a literature-known procedure.[4,23] The solution colour immediately changed to an intense violet. The solvent was removed under reduced pressure to give **FcDurSXanth$^{CF_{3+}}$** in quantitative yield as a brown solid.

ESI-MS *calc*. for $C_{35}H_{27}F_6FeS^+$ $\frac{m}{z}$ = 649.1082 (M^+); *found* 649.1090 (measured in CH_2Cl_2, calibrated).

Elemental Analysis *calcd*. for $C_{67}H_{39}BF_{30}FeS$: 53.20% C, 2.60% H; *found* 53.04% C, 3.08% H.

NMR spectroscopy and mass spectrometry

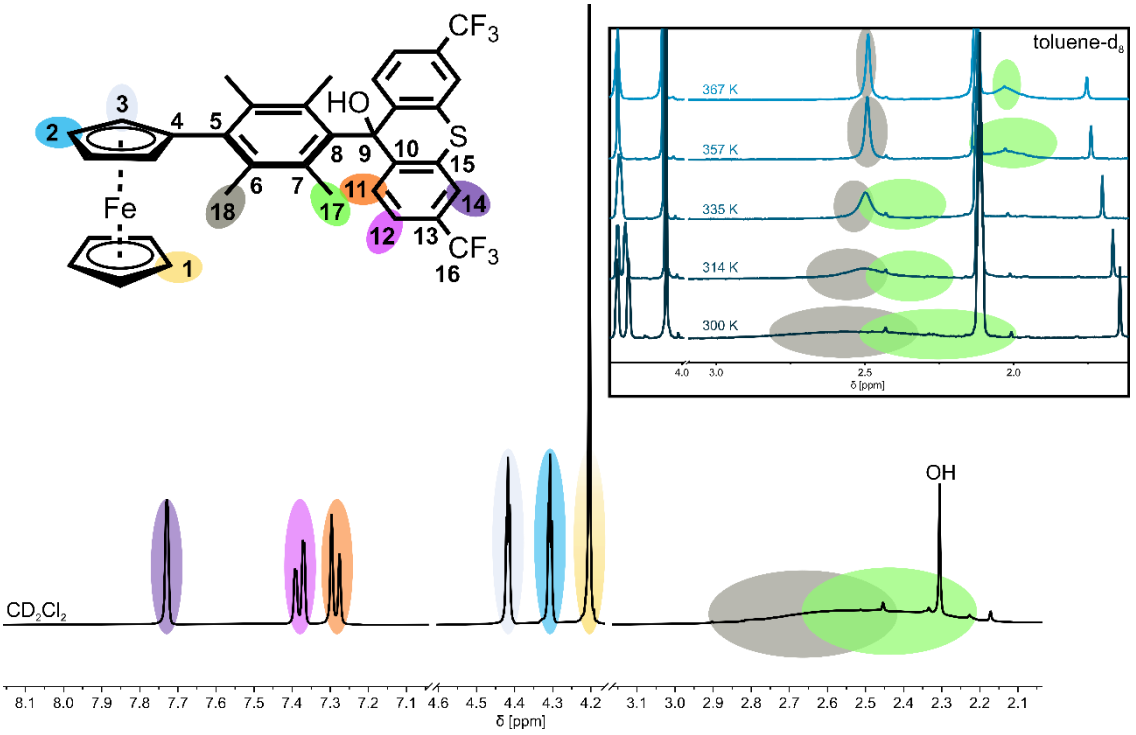

Figure S1 | ^{1}H-NMR spectrum of **FcDurSXanth^{CF_3}-OH** in CD_2Cl_2 at 298 K; insert: *T*-dependent ^{1}H-NMR spectra (400 MHz) from 300 K (±0.1 K) to 367 K (±0.1 K) in toluene-d$_8$.

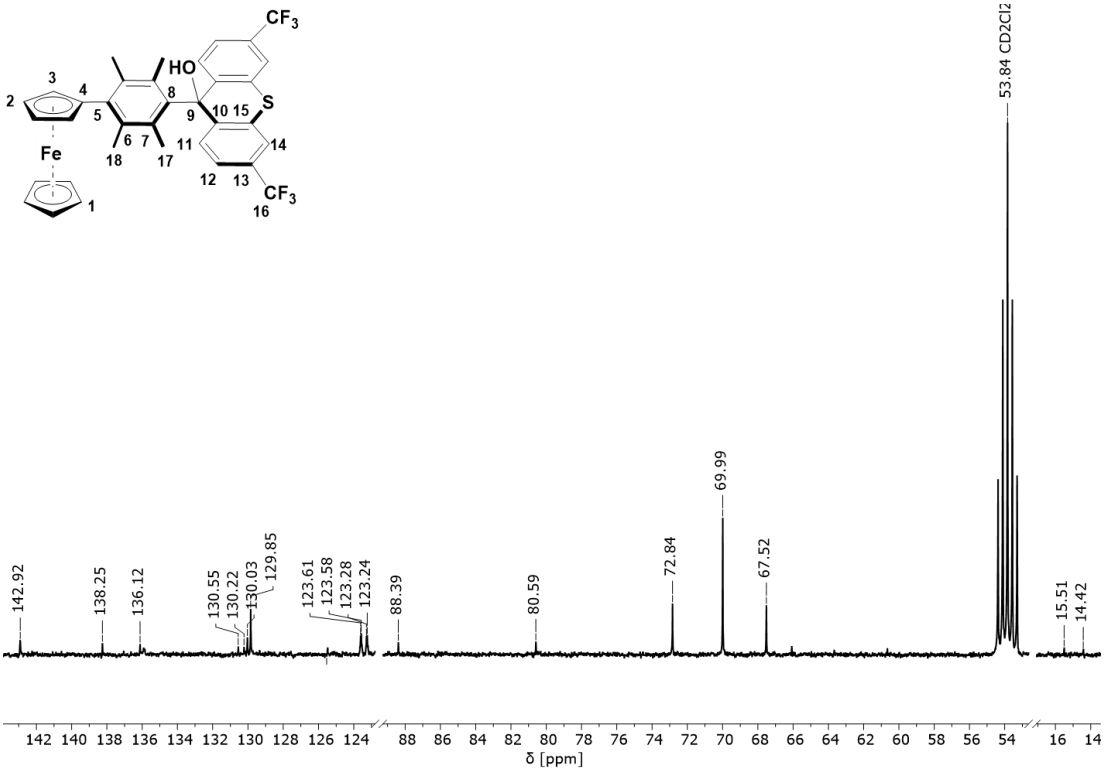

Figure S2 | ^{13}C{^{1}H}-NMR spectrum of compound **FcDurSXanth^{CF_3}-OH** measured in CD_2Cl_2.

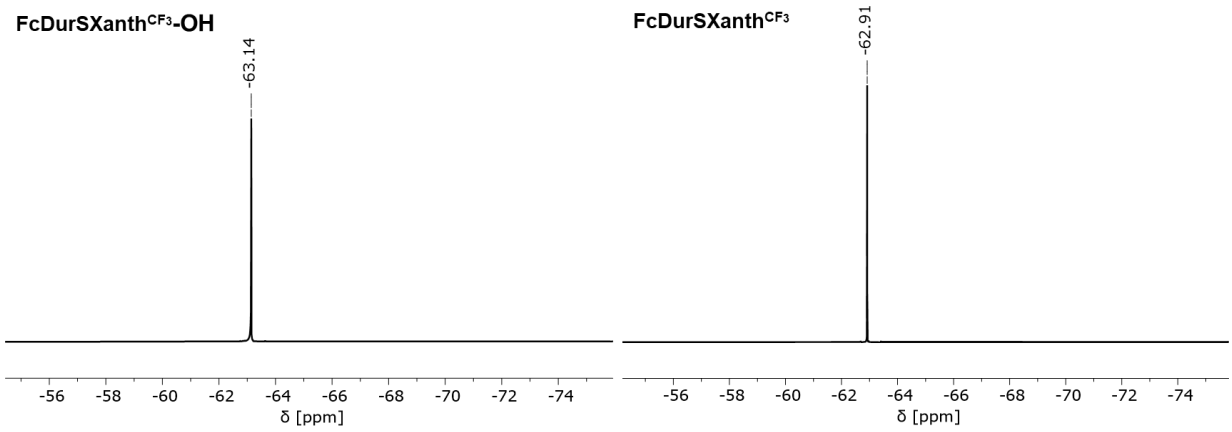

Figure S3 | $^{19}F\{^{1}H\}$-NMR (376 MHz) spectra of the carbinol precursor **FcDurSXanth^{CF_3}-OH** (left) and the respective cation **FcDurSXanth^{CF_3}** (right).

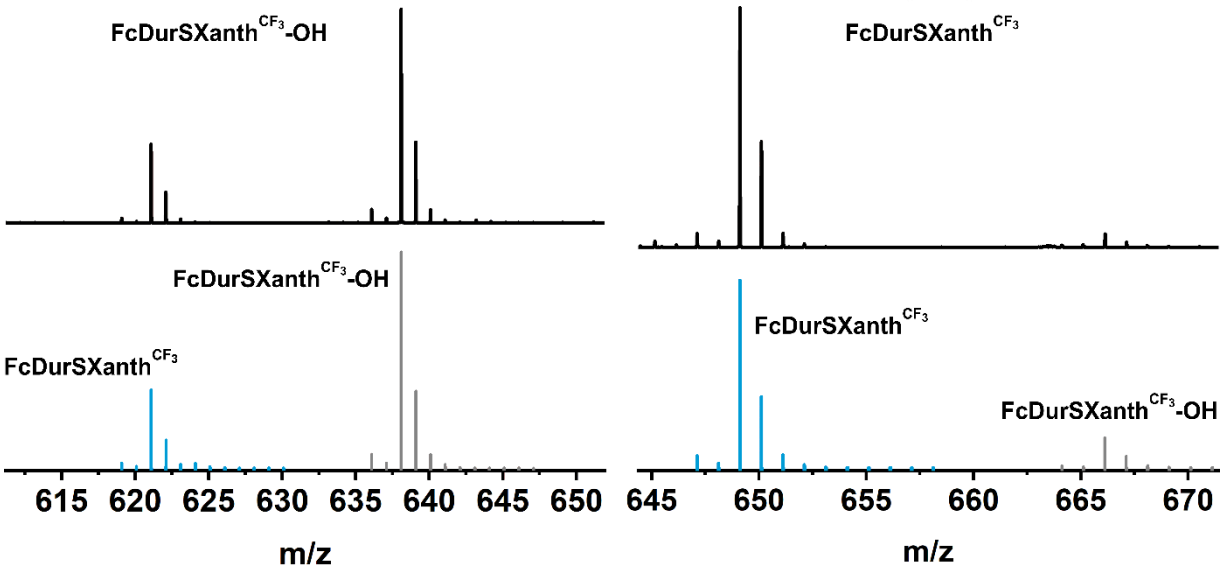

Figure S4 | Experimental (black) and simulated (blue, cation; grey, carbinol) data from mass spectrometry of **FcDurSXanth^{CF_3}** and **FcDurSXanth^{CF_3}-OH**.

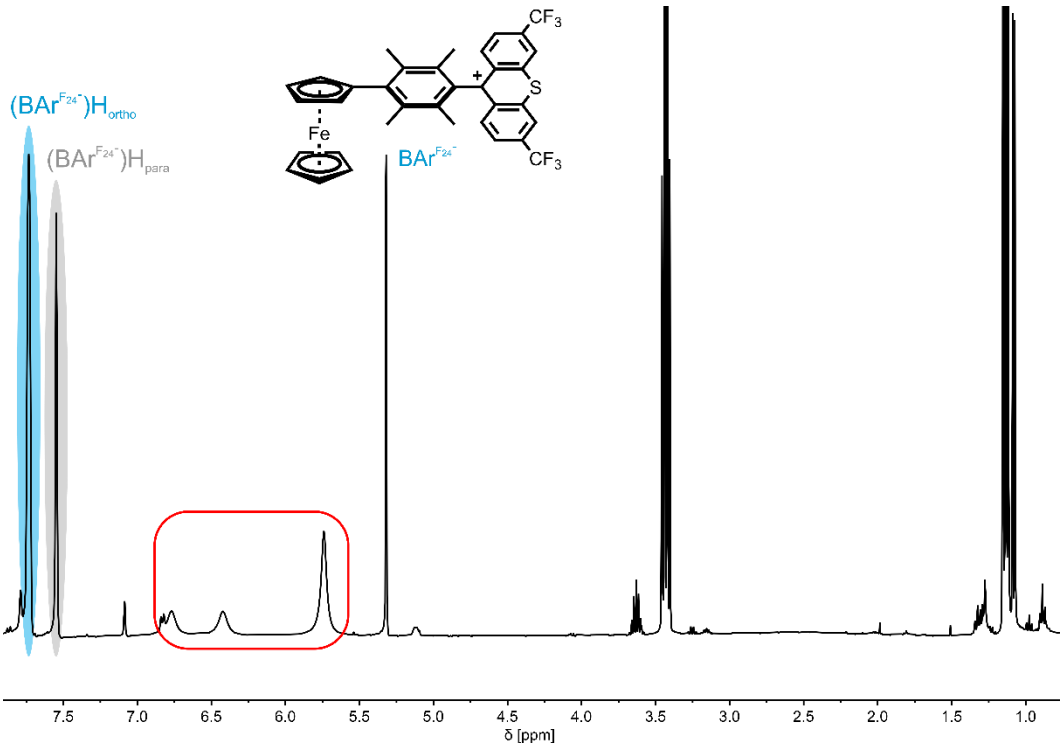

Figure S5 | ^{1}H-NMR spectrum of **FcDurSXanth$^{CF_3+}$** in CD_2Cl_2 at 298 K.

UV-Vis-NIR Spectroscopy

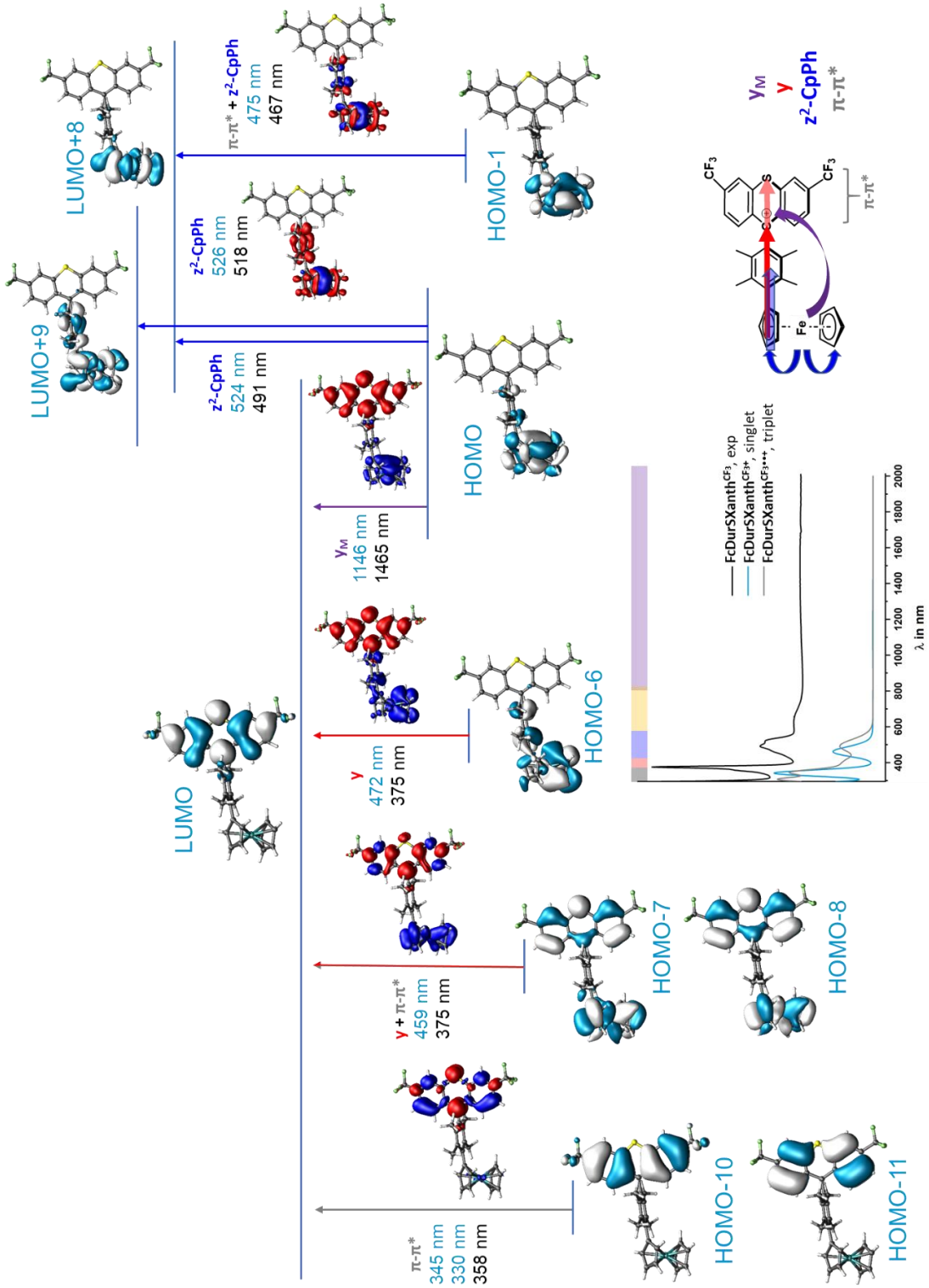

Figure S6 | TD-DFT-computed molecular orbital contributions to major transitions calculated for complex **FcDurSXanth$^{CF_3+}$** with EDDMs (electron density difference maps, blue: electron loss, red: electron gain). The experimental (TD-DFT calculated) spectrum and data given in black (blue).

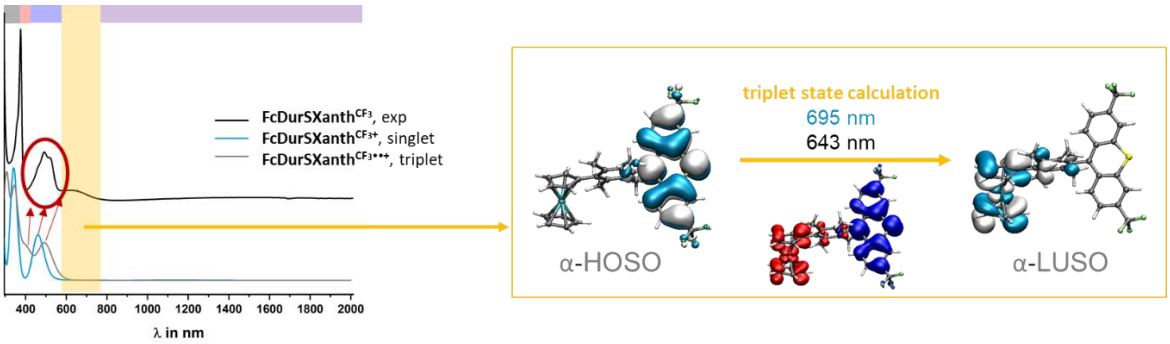

Figure S7 | TD-DFT computed and experimental UV/Vis/NIR spectra (left) and the α-HOSO to α-LUSO transition of the triplet state of the diradical valence tautomer of **FcDurSXanth$^{CF_3+}$** (right). For the EDDM plots, blue/red colors indicate a loss/gain of electron density.

Cyclic Voltammetry

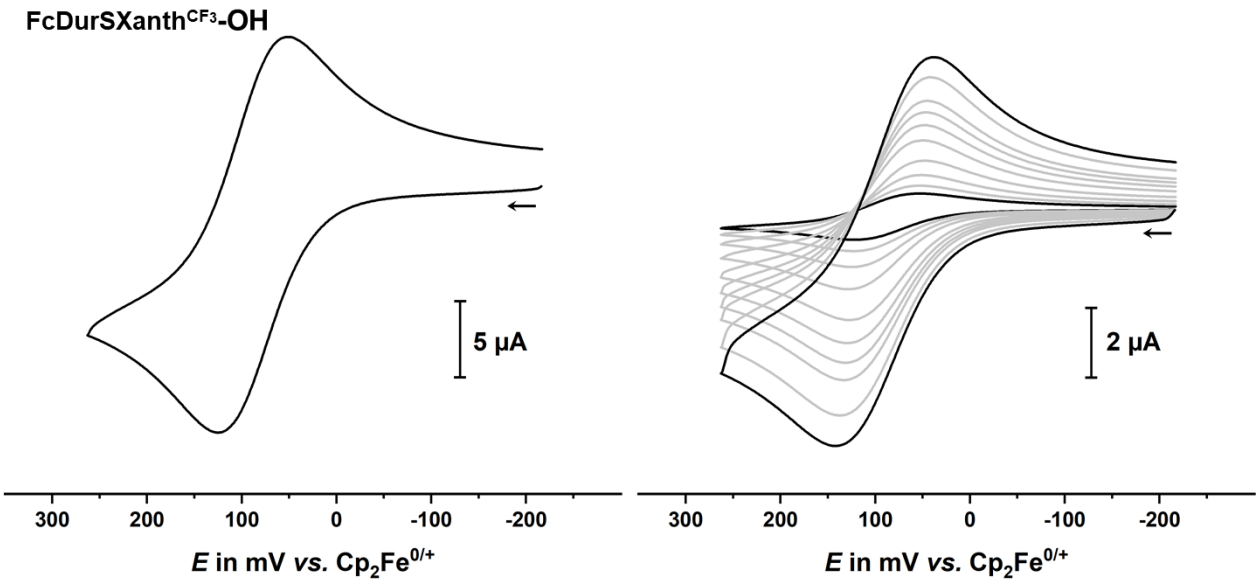

Figure S8 | Cyclic voltammograms of **FcDurSXanth^{CF_3}-OH** between (0.1 mM $^{n}Bu_4N^+BAr^{F_{24}-}$) measured at a scan rate of 100 mVs^{-1} (left) and at different scan rates ranging from 25 mVs^{-1} to 2000 mVs^{-1} (right).

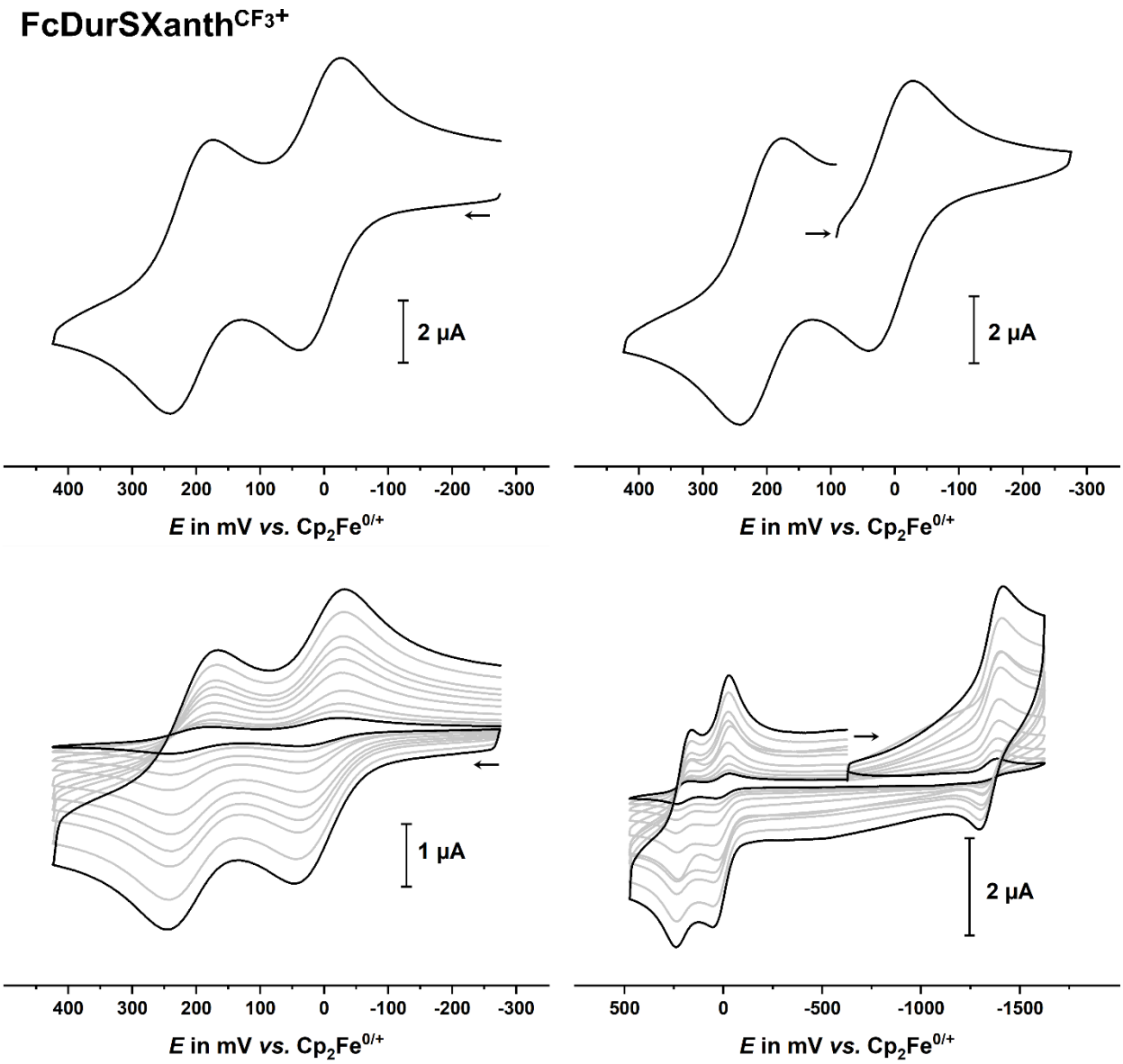

Figure S9 | Cyclic voltammograms of **FcDurSXanth$^{CF_3+}$** (0.1 mM $^{n}Bu_4N^{+}BAr^{F_{24}-}$) measured at a scan rate of 100 mVs^{-1} (upper part) and at different scan rates ranging from 25 mVs^{-1} to 2000 mVs^{-1} (bottom). The figure on the top right shows a scan initiated from the resting potential.

Table S1 | Electrochemical data of the complex cation **FcDurSXanth^{CF_3}** $^{+}$ (in 0.1 mM $^{n}Bu_4N^{+}BAr^{F_{24}-}$ in CH_2Cl_2).

Scan rate [mVs^{-1}]	$E_{1/2}^{+/2+}$ [mV]	ΔE_p [mV]	$E_{1/2}^{+/0}$ [mV]	ΔE_p [mV]	$E_{1/2}^{0/-}$ [mV]	ΔE_p [mV]
25	215	65	15	60	-1330	65
50	210	70	10	60	-1340	60
100	205	75	5	60	-1345	70
200	200	75	5	65	-1355	85
400	195	65	5	75	-1355	80
600	190	65	-15	55	-1360	90
800	205	65	15	70	-1350	90
1000	200	70	5	70	-1355	100
1500	185	70	-5	75	-1370	105
2000	190	80	-5	75	-1370	115

X-ray crystallography

Table S2 | Crystal data and structure refinement for **FcDurSXanth$^{CF_3+}$** $BAr^{F_{24}-}$.

Empirical formula	$C_{67}H_{39}BF_{30}FeS$
Formula weight	1512.70
Temperature/K	100.0
Crystal system	triclinic
Space group	$P\bar{1}$
a/Å	11.9778(3)
b/Å	12.5044(3)
c/Å	21.1080(6)
α/°	80.916(2)
β/°	75.471(2)
γ/°	85.239(2)
Volume/Å^3	3018.86(14)
Z	2
ρ_{calc}g/cm^3	1.664
μ/mm^{-1}	0.422
F(000)	1516.0
Crystal size/mm^3	0.35 × 0.06 × 0.06
Radiation	MoKα (λ = 0.71073)
2Θ range for data collection/°	5.954 to 55.114
Index ranges	$-15 \le h \le 15$, $-16 \le k \le 14$, $-27 \le l \le 27$
Reflections collected	31264
Independent reflections	13839 [R_{int} = 0.0287, R_{sigma} = 0.0423]
Data/restraints/parameters	13839/0/906
Goodness-of-fit on F^2	1.088
Final R indexes [$I \ge 2\sigma(I)$]	R_1 = 0.0461, wR_2 = 0.1094
Final R indexes [all data]	R_1 = 0.0814, wR_2 = 0.1394
Largest diff. peak/hole / e Å^{-3}	0.73/-0.75

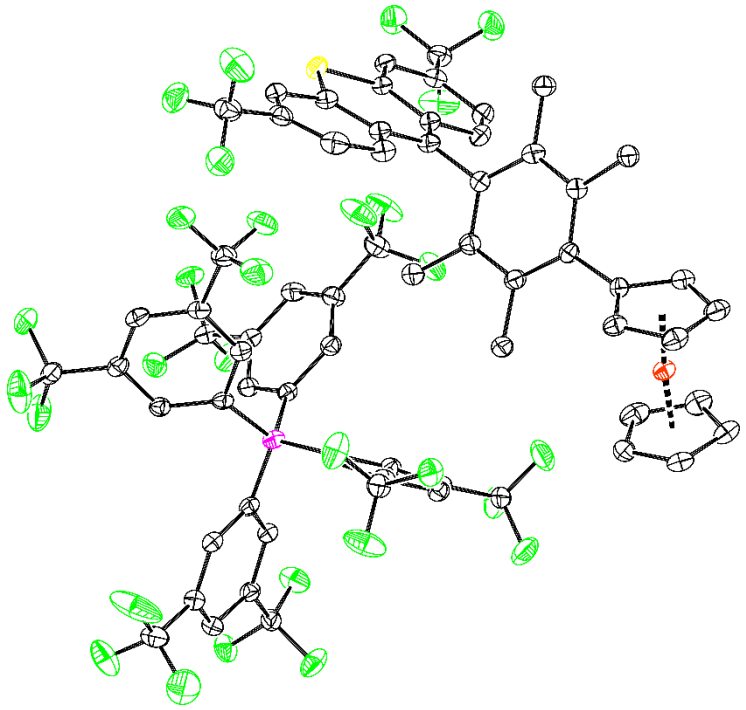

Figure S10 | ORTEP of **FcDurSXanth**$^{CF_3+}$ $BAr^{F_{24}-}$. Hydrogen atoms are omitted for reasons of clarity. Ellipsoids are displayed at a 50% probability level.

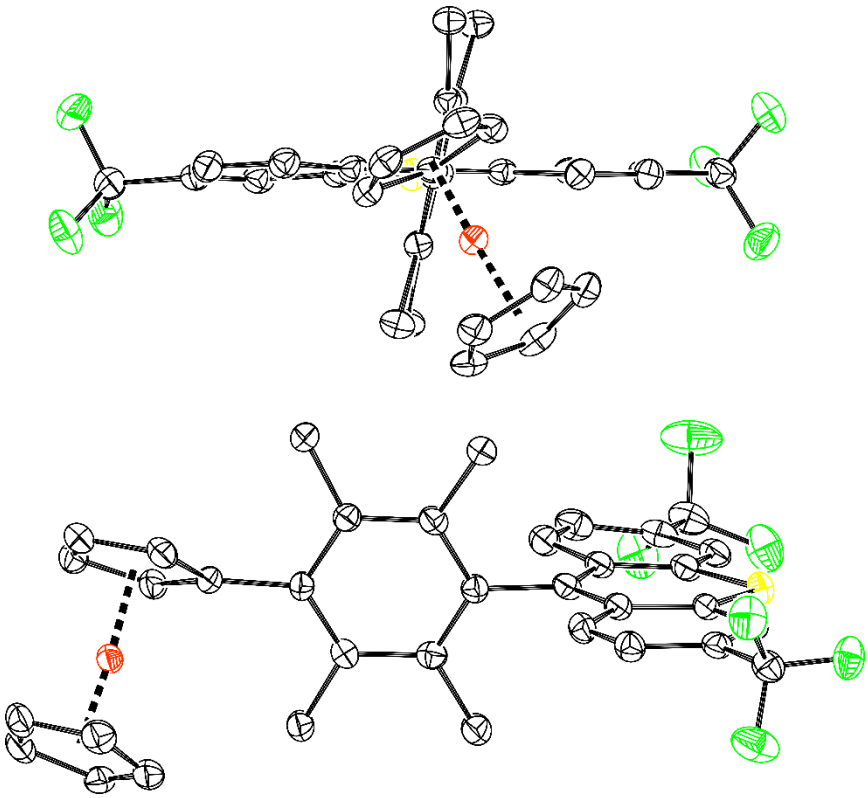

Figure 11 | Two different perspective views of the complex cation **FcDurSXanth**$^{CF_3+}$ in the $BAr^{F_{24}-}$ salt. Ellipsoids are drawn at the 50% probability level. Hydrogen atoms and counter anion are omitted for reasons of clarity.

Table S3 | Crystallographically determined bond lengths of **FcDurSXanth$^{CF_3+}$ BAr$^{F_{24}-}$**.

Atom	Atom	Length/Å	Atom	Atom	Length/Å
Fe1	C36	2.051(3)	F9	C31	1.345(3)
Fe1	C37	2.040(3)	F10	C8	1.336(3)
Fe1	C38	2.042(3)	F11	C8	1.340(3)
Fe1	C39	2.043(3)	F12	C8	1.352(4)
Fe1	C40	2.044(3)	F13	C32	1.339(4)
Fe1	C41	2.032(3)	F14	C23	1.330(4)
Fe1	C42	2.027(3)	F15	C31	1.330(3)
Fe1	C43	2.035(3)	F16	C23	1.346(4)
Fe1	C44	2.053(3)	F17	C32	1.346(3)
Fe1	C45	2.084(3)	F18	C7	1.334(3)
S1	C63	1.701(3)	F19	C7	1.323(3)
S1	C64	1.704(3)	F20	C23	1.333(4)
F1	C61	1.324(4)	F21	C16	1.329(4)
F2	C61	1.341(4)	F22	C7	1.331(3)
F3	C61	1.329(4)	F23	C16	1.331(4)
F4	C67	1.337(3)	F24	C16	1.307(4)
F5	C67	1.323(3)	F25	C24	1.343(3)
F6	C67	1.333(3)	F26	C15	1.346(3)
C33	C34	1.359(4)	F27	C32	1.332(3)
C33	C66	1.408(4)	F28	C24	1.345(3)
C34	C35	1.424(4)	F29	C24	1.350(3)
C35	C56	1.412(4)	F30	C31	1.327(3)
C35	C64	1.421(4)	C1	C2	1.398(4)
C36	C37	1.414(4)	C1	C6	1.398(4)
C36	C40	1.417(4)	C1	B1	1.639(4)
C37	C38	1.422(4)	C2	C3	1.389(4)
C38	C39	1.416(4)	C3	C4	1.381(4)
C39	C40	1.402(4)	C3	C8	1.490(4)
C41	C42	1.419(4)	C4	C5	1.391(4)
C41	C45	1.429(4)	C5	C6	1.389(4)
C42	C43	1.417(4)	C5	C7	1.491(4)
C43	C44	1.424(4)	C9	C10	1.397(4)
C44	C45	1.419(4)	C9	C14	1.398(4)
C45	C46	1.501(4)	C9	B1	1.637(4)
C46	C47	1.416(4)	C10	C11	1.386(4)
C46	C54	1.401(4)	C11	C12	1.390(4)
C47	C48	1.517(4)	C11	C16	1.495(4)
C47	C49	1.393(4)	C12	C13	1.392(4)
C49	C50	1.514(4)	C13	C14	1.393(4)
C49	C51	1.400(4)	C13	C15	1.491(4)
C51	C52	1.398(4)	C17	C18	1.404(4)
C51	C56	1.496(4)	C17	C22	1.395(4)
C52	C53	1.507(4)	C17	B1	1.628(4)
C52	C54	1.409(4)	C18	C19	1.383(4)
C54	C55	1.508(4)	C19	C20	1.400(4)
C56	C57	1.420(4)	C19	C24	1.483(4)
C57	C58	1.422(4)	C20	C21	1.381(4)
C57	C63	1.422(4)	C21	C22	1.395(4)
C58	C59	1.367(4)	C21	C23	1.482(4)
C59	C60	1.411(4)	C25	C26	1.399(4)
C60	C61	1.506(4)	C25	C30	1.409(4)
C60	C62	1.362(4)	C25	B1	1.632(4)
C62	C63	1.416(4)	C26	C27	1.387(4)
C64	C65	1.407(4)	C27	C28	1.389(4)
C65	C66	1.371(4)	C27	C32	1.489(4)
C66	C67	1.501(4)	C28	C29	1.389(4)
F7	C15	1.343(3)	C29	C30	1.389(4)
F8	C15	1.332(3)	C29	C31	1.493(4)

Table S4 | Crystallographically determined bond angles of **FcDurSXanth$^{CF_3+}$ BAr$^{F_{24}-}$**.

Atom	Atom	Atom	Angle/°	Atom	Atom	Atom	Angle/°
C36	Fe1	C44	129.93(12)	C60	C62	C63	118.9(3)
C36	Fe1	C45	112.36(11)	C57	C63	S1	123.9(2)
C37	Fe1	C36	40.44(13)	C62	C63	S1	115.3(2)
C37	Fe1	C38	40.76(12)	C62	C63	C57	120.9(3)
C37	Fe1	C39	68.36(13)	C35	C64	S1	124.1(2)
C37	Fe1	C40	68.09(13)	C65	C64	S1	114.9(2)
C37	Fe1	C44	165.03(12)	C65	C64	C35	121.0(2)
C37	Fe1	C45	126.75(12)	C66	C65	C64	119.0(3)
C38	Fe1	C36	68.07(12)	C33	C66	C67	118.6(3)
C38	Fe1	C39	40.57(12)	C65	C66	C33	121.4(3)
C38	Fe1	C40	67.84(12)	C65	C66	C67	120.0(3)
C38	Fe1	C44	154.13(12)	F4	C67	C66	110.8(2)
C38	Fe1	C45	160.67(12)	F5	C67	F4	107.5(2)
C39	Fe1	C36	67.97(12)	F5	C67	F6	107.4(2)
C39	Fe1	C40	40.11(12)	F5	C67	C66	112.8(2)
C39	Fe1	C44	122.15(12)	F6	C67	F4	106.7(2)
C39	Fe1	C45	158.70(12)	F6	C67	C66	111.4(2)
C40	Fe1	C36	40.49(12)	C2	C1	B1	120.0(2)
C40	Fe1	C44	112.10(12)	C6	C1	C2	115.5(2)
C40	Fe1	C45	125.99(11)	C6	C1	B1	123.4(2)
C41	Fe1	C36	122.26(13)	C3	C2	C1	122.6(3)
C41	Fe1	C37	106.05(13)	C2	C3	C8	118.0(3)
C41	Fe1	C38	121.61(12)	C4	C3	C2	120.6(2)
C41	Fe1	C39	158.26(12)	C4	C3	C8	121.3(3)
C41	Fe1	C40	159.21(12)	C3	C4	C5	118.3(2)
C41	Fe1	C43	68.67(12)	C4	C5	C7	119.0(2)
C41	Fe1	C44	68.18(12)	C6	C5	C4	120.4(2)
C41	Fe1	C45	40.59(11)	C6	C5	C7	120.5(2)
C42	Fe1	C36	154.17(13)	C5	C6	C1	122.6(2)
C42	Fe1	C37	116.89(13)	F18	C7	C5	112.5(2)
C42	Fe1	C38	102.48(13)	F19	C7	F18	105.4(2)
C42	Fe1	C39	121.24(12)	F19	C7	F22	105.9(3)
C42	Fe1	C40	159.79(12)	F19	C7	C5	113.8(2)
C42	Fe1	C41	40.94(12)	F22	C7	F18	105.5(2)
C42	Fe1	C43	40.84(12)	F22	C7	C5	113.0(2)
C42	Fe1	C44	68.49(12)	F10	C8	F11	106.6(2)
C42	Fe1	C45	68.42(11)	F10	C8	F12	106.0(2)
C43	Fe1	C36	164.97(13)	F10	C8	C3	113.6(3)
C43	Fe1	C37	151.71(13)	F11	C8	F12	105.0(2)
C43	Fe1	C38	116.73(12)	F11	C8	C3	112.2(2)
C43	Fe1	C39	105.76(12)	F12	C8	C3	112.8(2)
C43	Fe1	C40	126.13(13)	C10	C9	C14	116.5(2)
C43	Fe1	C44	40.79(11)	C10	C9	B1	121.1(2)
C43	Fe1	C45	68.22(11)	C14	C9	B1	122.2(2)
C44	Fe1	C45	40.12(11)	C11	C10	C9	122.0(3)
C63	S1	C64	103.97(14)	C10	C11	C12	120.8(3)
C34	C33	C66	119.9(3)	C10	C11	C16	120.4(3)
C33	C34	C35	121.5(3)	C12	C11	C16	118.8(2)
C56	C35	C34	120.3(2)	C11	C12	C13	118.2(2)
C56	C35	C64	122.5(2)	C12	C13	C14	120.6(3)
C64	C35	C34	117.3(3)	C12	C13	C15	118.2(2)
C37	C36	Fe1	69.37(17)	C14	C13	C15	121.2(2)
C37	C36	C40	107.7(3)	C13	C14	C9	121.9(3)
C40	C36	Fe1	69.51(17)	F7	C15	F26	105.5(2)
C36	C37	Fe1	70.18(17)	F7	C15	C13	112.0(2)
C36	C37	C38	107.8(3)	F8	C15	F7	106.8(2)
C38	C37	Fe1	69.69(17)	F8	C15	F26	106.3(2)
C37	C38	Fe1	69.56(16)	F8	C15	C13	113.3(2)
C39	C38	Fe1	69.74(17)	F26	C15	C13	112.5(2)
C39	C38	C37	107.9(3)	F21	C16	F23	103.8(3)
C38	C39	Fe1	69.69(16)	F21	C16	C11	113.0(3)
C40	C39	Fe1	70.00(16)	F23	C16	C11	111.6(3)
C40	C39	C38	108.0(3)	F24	C16	F21	105.9(3)
C36	C40	Fe1	70.01(17)	F24	C16	F23	107.8(3)
C39	C40	Fe1	69.88(16)	F24	C16	C11	114.1(2)
C39	C40	C36	108.5(3)	C18	C17	B1	121.4(2)
C42	C41	Fe1	69.33(16)	C22	C17	C18	115.7(2)
C42	C41	C45	108.5(3)	C22	C17	B1	121.5(2)
C45	C41	Fe1	71.67(15)	C19	C18	C17	122.5(2)
C41	C42	Fe1	69.74(17)	C18	C19	C20	120.5(3)
C43	C42	Fe1	69.89(17)	C18	C19	C24	120.5(2)
C43	C42	C41	107.9(3)	C20	C19	C24	119.0(2)
C42	C43	Fe1	69.27(17)	C21	C20	C19	118.1(3)

C42	C43	C44	107.8(3)	C20	C21	C22	120.7(3)
C44	C43	Fe1	70.29(16)	C20	C21	C23	120.7(3)
C43	C44	Fe1	68.93(17)	C22	C21	C23	118.4(3)
C45	C44	Fe1	71.14(16)	C21	C22	C17	122.4(3)
C45	C44	C43	108.7(3)	F14	C23	F16	105.6(2)
C41	C45	Fe1	67.73(15)	F14	C23	F20	106.8(3)
C41	C45	C46	124.4(2)	F14	C23	C21	113.6(3)
C44	C45	Fe1	68.74(15)	F16	C23	C21	111.9(3)
C44	C45	C41	107.0(2)	F20	C23	F16	105.2(3)
C44	C45	C46	127.7(2)	F20	C23	C21	113.1(2)
C46	C45	Fe1	136.78(19)	F25	C24	F28	106.0(2)
C47	C46	C45	117.0(2)	F25	C24	F29	106.0(2)
C54	C46	C45	123.3(2)	F25	C24	C19	113.0(2)
C54	C46	C47	119.6(2)	F28	C24	F29	105.6(2)
C46	C47	C48	121.5(2)	F28	C24	C19	113.0(2)
C49	C47	C46	120.5(2)	F29	C24	C19	112.6(2)
C49	C47	C48	117.9(2)	C26	C25	C30	115.9(2)
C47	C49	C50	120.7(2)	C26	C25	B1	123.0(2)
C47	C49	C51	118.8(2)	C30	C25	B1	120.8(2)
C51	C49	C50	120.5(2)	C27	C26	C25	122.6(3)
C49	C51	C56	119.5(2)	C26	C27	C28	120.3(3)
C52	C51	C49	121.9(2)	C26	C27	C32	119.8(3)
C52	C51	C56	118.2(2)	C28	C27	C32	119.9(2)
C51	C52	C53	121.8(2)	C29	C28	C27	118.6(3)
C51	C52	C54	118.8(2)	C28	C29	C30	120.7(3)
C54	C52	C53	119.4(2)	C28	C29	C31	118.7(2)
C46	C54	C52	120.2(2)	C30	C29	C31	120.6(3)
C46	C54	C55	122.6(2)	C29	C30	C25	121.9(3)
C52	C54	C55	117.2(2)	F9	C31	C29	111.4(2)
C35	C56	C51	119.9(2)	F15	C31	F9	106.3(2)
C35	C56	C57	122.8(3)	F15	C31	C29	112.4(2)
C57	C56	C51	117.3(2)	F30	C31	F9	105.5(2)
C56	C57	C58	120.0(3)	F30	C31	F15	106.9(2)
C56	C57	C63	122.5(3)	F30	C31	C29	113.7(2)
C58	C57	C63	117.5(3)	F13	C32	F17	105.6(3)
C59	C58	C57	120.9(3)	F13	C32	C27	113.0(2)
C58	C59	C60	120.1(3)	F17	C32	C27	111.9(2)
C59	C60	C61	118.6(3)	F27	C32	F13	106.4(2)
C62	C60	C59	121.4(3)	F27	C32	F17	106.1(2)
C62	C60	C61	119.9(3)	F27	C32	C27	113.2(2)
F1	C61	F2	107.6(3)	C9	B1	C1	113.1(2)
F1	C61	F3	106.8(3)	C17	B1	C1	100.3(2)
F1	C61	C60	111.5(3)	C17	B1	C9	114.7(2)
F2	C61	C60	110.8(3)	C17	B1	C25	112.7(2)
F3	C61	F2	106.6(2)	C25	B1	C1	112.4(2)
F3	C61	C60	113.2(3)	C25	B1	C9	104.0(2)

Table 5 | Crystallographically determined torsion angles of **FcDurSXanth$^{CF_3+}$ BAr$^{F_{24}-}$**.

A	B	C	D	Angle/°	A	B	C	D	Angle/°
Fe1	C36	C37	C38	59.8(2)	C1	C2	C3	C8	-175.7(3)
Fe1	C36	C40	C39	-59.5(2)	C2	C1	C6	C5	-0.6(4)
Fe1	C37	C38	C39	59.4(2)	C2	C1	B1	C9	162.7(2)
Fe1	C38	C39	C40	59.7(2)	C2	C1	B1	C17	-74.6(3)
Fe1	C39	C40	C36	59.5(2)	C2	C1	B1	C25	45.3(3)
Fe1	C41	C42	C43	-59.7(2)	C2	C3	C4	C5	-1.8(4)
Fe1	C41	C45	C44	57.65(19)	C2	C3	C8	F10	177.6(2)
Fe1	C41	C45	C46	-132.4(3)	C2	C3	C8	F11	56.6(4)
Fe1	C42	C43	C44	-60.0(2)	C2	C3	C8	F12	-61.8(3)
Fe1	C43	C44	C45	-60.27(19)	C3	C4	C5	C6	0.5(4)
Fe1	C44	C45	C41	-57.03(19)	C3	C4	C5	C7	-176.3(3)
Fe1	C44	C45	C46	133.4(3)	C4	C3	C8	F10	-0.1(4)
Fe1	C45	C46	C47	-140.0(2)	C4	C3	C8	F11	-121.1(3)
Fe1	C45	C46	C54	42.7(4)	C4	C3	C8	F12	120.5(3)
S1	C64	C65	C66	-177.0(2)	C4	C5	C6	C1	0.7(4)
C33	C34	C35	C56	-178.9(2)	C4	C5	C7	F18	46.1(4)
C33	C34	C35	C64	1.1(4)	C4	C5	C7	F19	165.9(3)
C33	C66	C67	F4	-55.6(3)	C4	C5	C7	F22	-73.2(3)
C33	C66	C67	F5	-176.1(2)	C6	C1	C2	C3	-0.7(4)
C33	C66	C67	F6	62.9(3)	C6	C1	B1	C9	-30.0(3)
C34	C33	C66	C65	-0.3(4)	C6	C1	B1	C17	92.6(3)
C34	C33	C66	C67	-179.3(2)	C6	C1	B1	C25	-147.4(2)
C34	C35	C56	C51	-0.9(4)	C6	C5	C7	F18	-130.7(3)
C34	C35	C56	C57	-179.8(2)	C6	C5	C7	F19	-10.9(4)
C34	C35	C64	S1	176.2(2)	C6	C5	C7	F22	110.0(3)
C34	C35	C64	C65	-1.4(4)	C7	C5	C6	C1	177.5(2)
C35	C56	C57	C58	-176.5(2)	C8	C3	C4	C5	175.9(3)
C35	C56	C57	C63	4.5(4)	C9	C10	C11	C12	0.8(4)
C35	C64	C65	C66	0.8(4)	C9	C10	C11	C16	-179.7(3)
C36	C37	C38	Fe1	-60.1(2)	C10	C9	C14	C13	1.1(4)
C36	C37	C38	C39	-0.7(3)	C10	C9	B1	C1	-39.1(3)
C37	C36	C40	Fe1	59.0(2)	C10	C9	B1	C17	-153.3(2)
C37	C36	C40	C39	-0.4(3)	C10	C9	B1	C25	83.2(3)
C37	C38	C39	Fe1	-59.3(2)	C10	C11	C12	C13	0.7(4)
C37	C38	C39	C40	0.4(3)	C10	C11	C16	F21	126.9(3)
C38	C39	C40	Fe1	-59.5(2)	C10	C11	C16	F23	-116.6(3)
C38	C39	C40	C36	0.0(3)	C10	C11	C16	F24	5.9(4)
C40	C36	C37	Fe1	-59.1(2)	C11	C12	C13	C14	-1.2(4)
C40	C36	C37	C38	0.7(3)	C11	C12	C13	C15	178.3(2)
C41	C42	C43	Fe1	59.6(2)	C12	C11	C16	F21	-53.5(4)
C41	C42	C43	C44	-0.4(3)	C12	C11	C16	F23	63.0(4)
C41	C45	C46	C47	-46.7(4)	C12	C11	C16	F24	-174.5(3)
C41	C45	C46	C54	136.0(3)	C12	C13	C14	C9	0.3(4)
C42	C41	C45	Fe1	-59.78(19)	C12	C13	C15	F7	-73.4(3)
C42	C41	C45	C44	-2.1(3)	C12	C13	C15	F8	165.7(2)
C42	C41	C45	C46	167.8(2)	C12	C13	C15	F26	45.1(3)
C42	C43	C44	Fe1	59.3(2)	C14	C9	C10	C11	-1.6(4)
C42	C43	C44	C45	-0.9(3)	C14	C9	B1	C1	146.8(2)
C43	C44	C45	Fe1	58.91(19)	C14	C9	B1	C17	32.5(4)
C43	C44	C45	C41	1.9(3)	C14	C9	B1	C25	-91.0(3)
C43	C44	C45	C46	-167.7(3)	C14	C13	C15	F7	106.1(3)
C44	C45	C46	C47	121.2(3)	C14	C13	C15	F8	-14.8(4)
C44	C45	C46	C54	-56.1(4)	C14	C13	C15	F26	-135.3(3)
C45	C41	C42	Fe1	61.25(19)	C15	C13	C14	C9	-179.2(2)
C45	C41	C42	C43	1.6(3)	C16	C11	C12	C13	-178.9(3)
C45	C46	C47	C48	-8.3(4)	C17	C18	C19	C20	0.7(4)
C45	C46	C47	C49	176.4(2)	C17	C18	C19	C24	-177.7(2)
C45	C46	C54	C52	179.9(3)	C18	C17	C22	C21	2.0(4)
C45	C46	C54	C55	1.7(4)	C18	C17	B1	C1	-80.0(3)
C46	C47	C49	C50	-174.4(3)	C18	C17	B1	C9	41.5(3)
C46	C47	C49	C51	6.1(4)	C18	C17	B1	C25	160.3(2)
C47	C46	C54	C52	2.7(4)	C18	C19	C20	C21	0.7(4)
C47	C46	C54	C55	-175.5(3)	C18	C19	C24	F25	144.4(3)
C47	C49	C51	C52	-2.8(4)	C18	C19	C24	F28	24.1(4)
C47	C49	C51	C56	169.6(3)	C18	C19	C24	F29	-95.5(3)
C48	C47	C49	C50	10.2(4)	C19	C20	C21	C22	-0.7(4)
C48	C47	C49	C51	-169.2(3)	C19	C20	C21	C23	-175.4(3)
C49	C51	C52	C53	-178.9(3)	C20	C19	C24	F25	-34.0(4)
C49	C51	C52	C54	-0.5(4)	C20	C19	C24	F28	-154.3(2)
C49	C51	C56	C35	82.6(3)	C20	C19	C24	F29	86.0(3)
C49	C51	C56	C57	-98.5(3)	C20	C21	C22	C17	-0.7(4)
C50	C49	C51	C52	177.7(3)	C20	C21	C23	F14	-16.4(4)
C50	C49	C51	C56	-9.9(4)	C20	C21	C23	F16	103.1(3)

C51	C52	C54	C46	0.6(4)	C20	C21	C23	F20	-138.3(3)
C51	C52	C54	C55	178.9(3)	C22	C17	C18	C19	-2.0(4)
C51	C56	C57	C58	4.6(4)	C22	C17	B1	C1	86.0(3)
C51	C56	C57	C63	-174.4(2)	C22	C17	B1	C9	-152.5(2)
C52	C51	C56	C35	-104.7(3)	C22	C17	B1	C25	-33.8(3)
C52	C51	C56	C57	74.2(3)	C22	C21	C23	F14	168.8(3)
C53	C52	C54	C46	179.0(3)	C22	C21	C23	F16	-71.8(4)
C53	C52	C54	C55	-2.7(4)	C22	C21	C23	F20	46.9(4)
C54	C46	C47	C48	169.1(3)	C23	C21	C22	C17	174.1(3)
C54	C46	C47	C49	-6.1(4)	C24	C19	C20	C21	179.1(3)
C56	C35	C64	S1	-3.8(4)	C25	C26	C27	C28	-0.9(4)
C56	C35	C64	C65	178.6(2)	C25	C26	C27	C32	-179.9(2)
C56	C51	C52	C53	8.6(4)	C26	C25	C30	C29	-0.1(4)
C56	C51	C52	C54	-173.0(3)	C26	C25	B1	C1	28.9(3)
C56	C57	C58	C59	-175.7(3)	C26	C25	B1	C9	-93.7(3)
C56	C57	C63	S1	-5.5(4)	C26	C25	B1	C17	141.4(2)
C56	C57	C63	C62	174.1(2)	C26	C27	C28	C29	0.4(4)
C57	C58	C59	C60	0.9(4)	C26	C27	C32	F13	-27.0(4)
C58	C57	C63	S1	175.5(2)	C26	C27	C32	F17	92.1(3)
C58	C57	C63	C62	-4.9(4)	C26	C27	C32	F27	-148.0(2)
C58	C59	C60	C61	178.1(3)	C27	C28	C29	C30	0.1(4)
C58	C59	C60	C62	-3.9(4)	C27	C28	C29	C31	179.3(2)
C59	C60	C61	F1	75.7(4)	C28	C27	C32	F13	154.0(2)
C59	C60	C61	F2	-44.1(4)	C28	C27	C32	F17	-86.9(3)
C59	C60	C61	F3	-163.8(3)	C28	C27	C32	F27	33.0(4)
C59	C60	C62	C63	2.3(4)	C28	C29	C30	C25	-0.3(4)
C60	C62	C63	S1	-178.2(2)	C28	C29	C31	F9	49.2(3)
C60	C62	C63	C57	2.1(4)	C28	C29	C31	F15	-70.1(3)
C61	C60	C62	C63	-179.7(3)	C28	C29	C31	F30	168.2(2)
C62	C60	C61	F1	-102.4(3)	C30	C25	C26	C27	0.7(4)
C62	C60	C61	F2	137.8(3)	C30	C25	B1	C1	-157.0(2)
C62	C60	C61	F3	18.2(4)	C30	C25	B1	C9	80.4(3)
C63	S1	C64	C35	2.5(3)	C30	C25	B1	C17	-44.5(3)
C63	S1	C64	C65	-179.79(19)	C30	C29	C31	F9	-131.6(3)
C63	C57	C58	C59	3.3(4)	C30	C29	C31	F15	109.1(3)
C64	S1	C63	C57	2.0(3)	C30	C29	C31	F30	-12.5(4)
C64	S1	C63	C62	-177.6(2)	C31	C29	C30	C25	-179.5(2)
C64	C35	C56	C51	179.1(2)	C32	C27	C28	C29	179.4(2)
C64	C35	C56	C57	0.2(4)	B1	C1	C2	C3	167.5(2)
C64	C65	C66	C33	0.0(4)	B1	C1	C6	C5	-168.4(2)
C64	C65	C66	C67	179.0(2)	B1	C9	C10	C11	-176.1(2)
C65	C66	C67	F4	125.3(3)	B1	C9	C14	C13	175.5(2)
C65	C66	C67	F5	4.8(4)	B1	C17	C18	C19	164.8(2)
C65	C66	C67	F6	-116.1(3)	B1	C17	C22	C21	-164.7(3)
C66	C33	C34	C35	-0.3(4)	B1	C25	C26	C27	175.1(2)
C1	C2	C3	C4	2.0(4)	B1	C25	C30	C29	-174.6(2)

Mößbauer and EPR spectroscopy

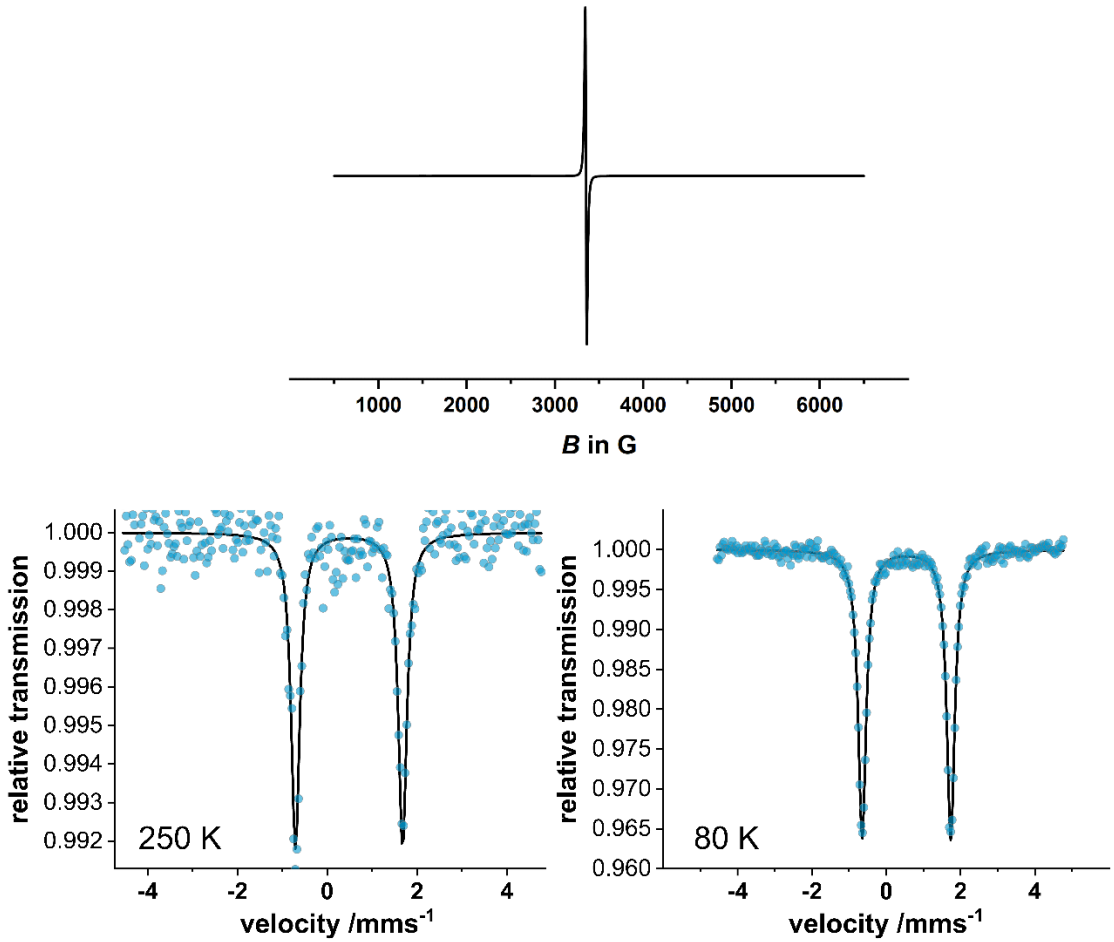

Figure S12 | Top: EPR spectrum of **FcDurSXanth**$^{CF_3+}$ $BAr^{F_{24}-}$ in frozen CH_2Cl_2 at 10 K. Bottom left: Mößbauer spectrum of a solid sample of **FcDurSXanth**$^{CF_3+}$ $BAr^{F_{24}-}$ at 250 K. Bottom right: Mößbauer spectrum of a solid sample of **FcDurSXanth**$^{CF_3+}$ $BAr^{F_{24}-}$ at 80 K.

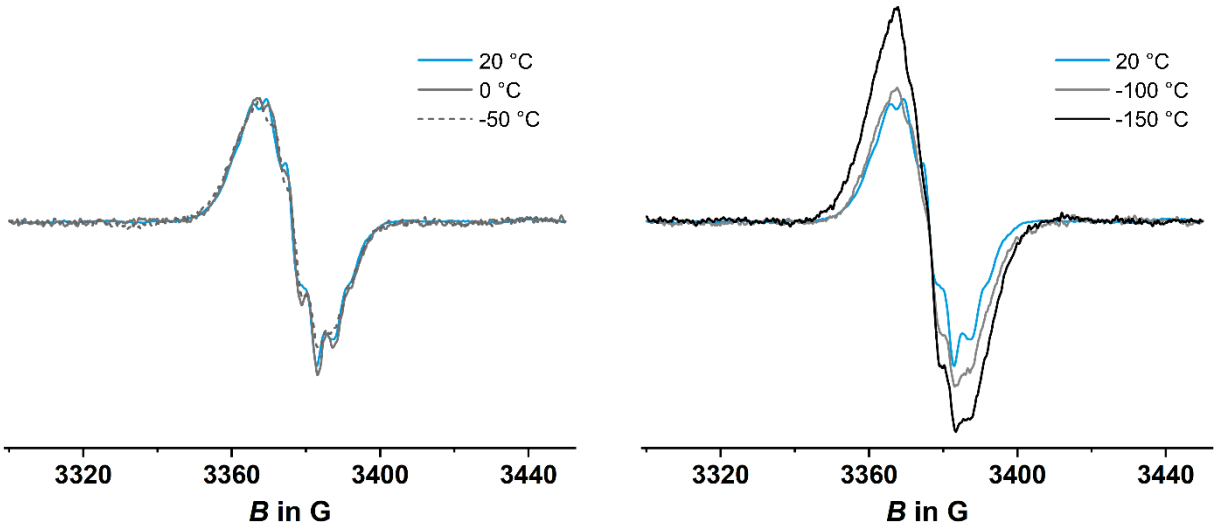

Figure S13 | *T*-dependent solid state EPR spectra of **FcDurSXanth**$^{CF_3+}$ recorded from a single crystalline sample.

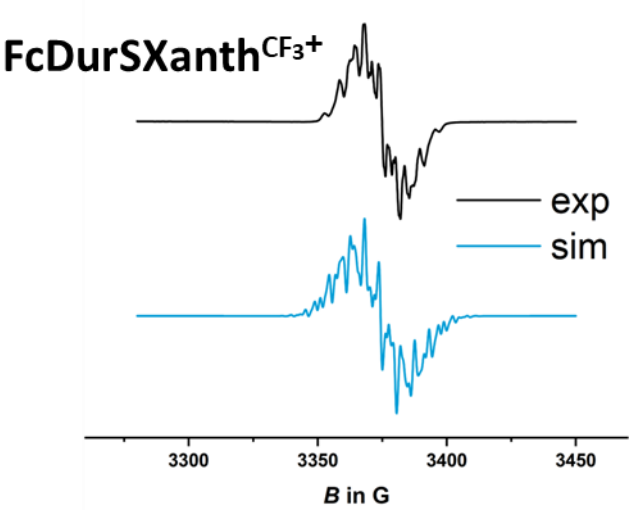

Figure S14 | Experimental EPR spectra (top, black) of cationic, diradical species of **FcDurSXanth**$^{CF_3+}$ (sample concentration 10 mM) in CH_2Cl_2 at 223 K including respective simulations (bottom, blue).

Table S6 | EPR spectroscopic data obtained by simulations.[24]

	T (°C)	*g*-value	*hfs* (^{1}H) in G[b]	*hfs* (^{1}H) in G[b]	*hfs* (^{1}H) in G[b]	*hfs* (^{1}H) in G[b]
FcDurSXanth^{CF3}[a]	-50	2.0047	16.0 (6)	15.0 (2)	12.8 (2)	9.8 (6)

[a] Diradical isomer content in the cationic species. [b] Number of equivalent protons in parentheses.

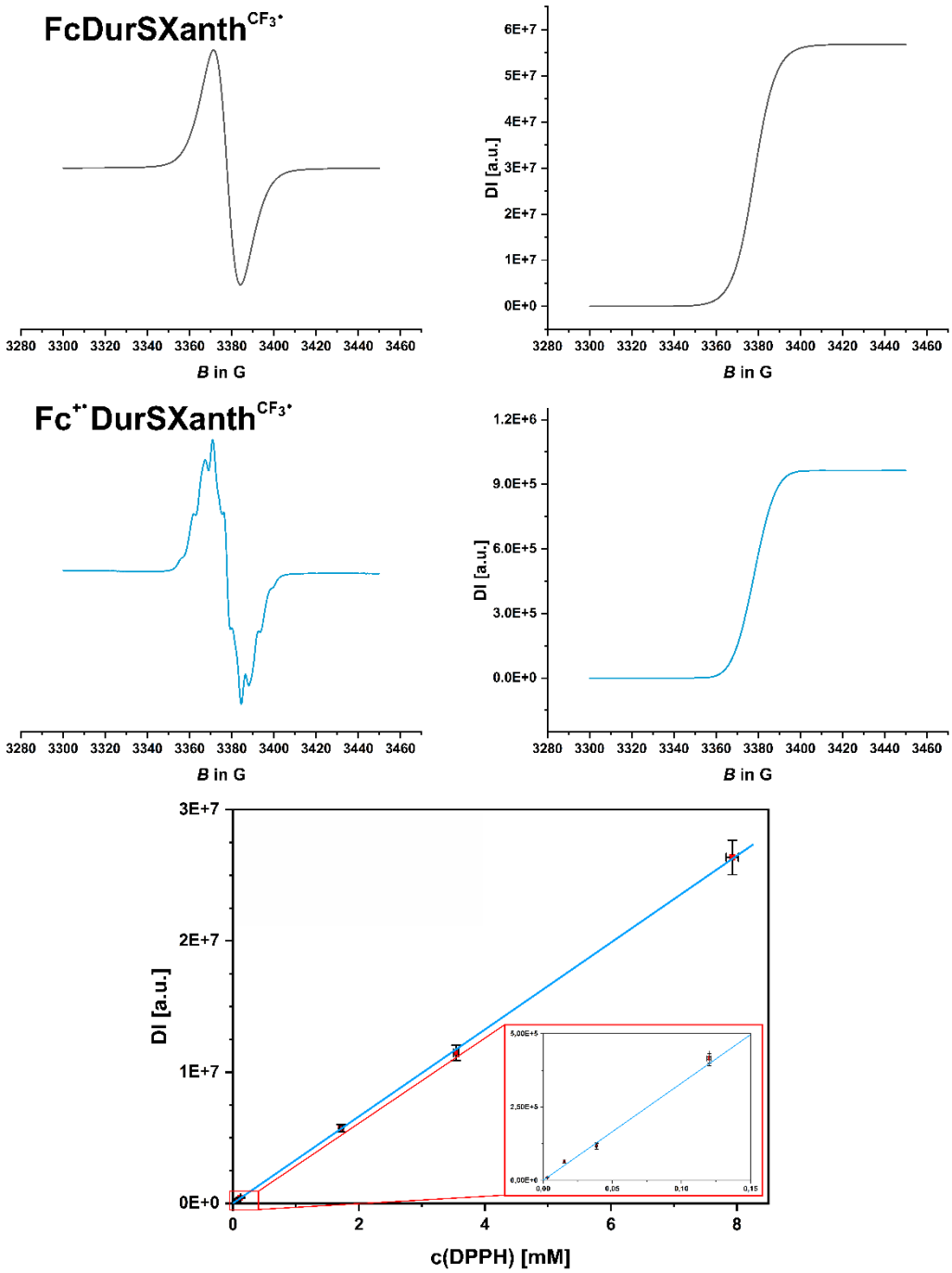

Figure S15 | Quantitative EPR spectroscopy. Top panel: EPR spectrum (left) of a CH_2Cl_2 solution of the **FcDurSXanth$^{CF_3\bullet}$** radical (*c* = 20 mM, *T* = 293 K) measured at standardized conditions and instrument settings; right: double integral of the EPR resonance signal. Middle panel: EPR spectrum (left) of a CH_2Cl_2 solution of **FcDurSXanth$^{CF_3+}$** $BAr^{F_{24}-}$ (*c* = 20 mM, *T* = 293 K) measured at standardized conditions and instrument settings; right: double integral of the EPR resonance signal. Value of the double integral of EPR spectra of CH_2Cl_2 solutions of variously concentrated solutions of the dpph$^\bullet$ radical standard at *T* = 293 K. The EPR spectra of the dpph$^\bullet$ standard were recorded under the same standardized conditions and instrument settings as above. For full details of the employed procedure, see ref. 6.

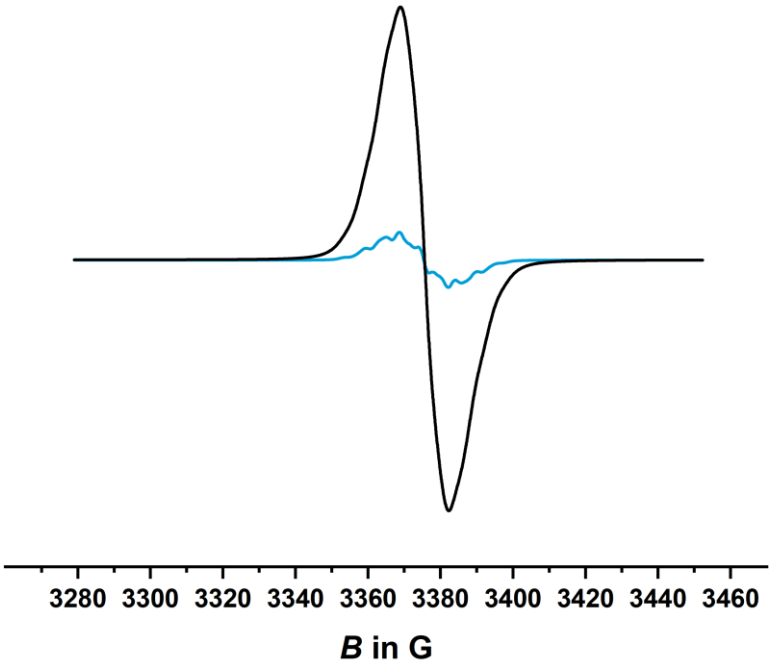

Figure S16 | Comparison of the EPR spectrum of a 10 M solution of the **FcDurSXanth**$^{CF_3+}$ cation (blue line) and of an equally concentrated solution of chemically reduced **FcDurSXanth**$^{CF_3\bullet}$ (black line) at *T* = 293 K.

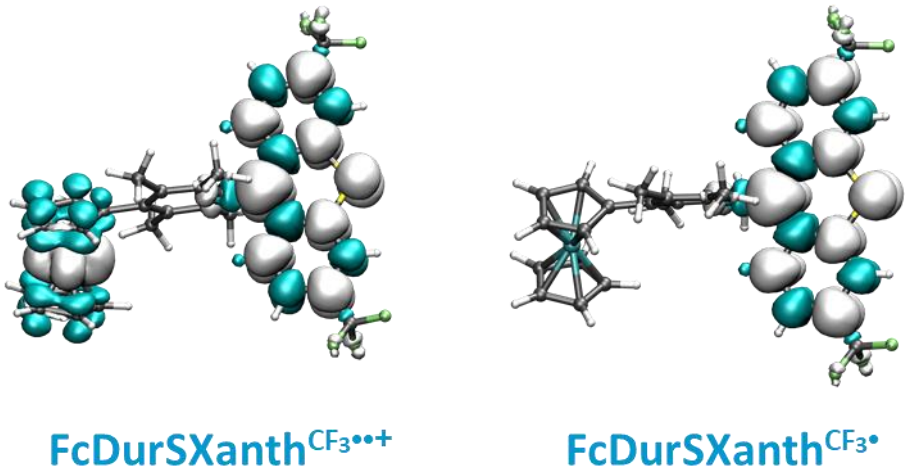

Figure S17 | DFT-calculated spin-density distributions for the diradical valence tautomer of **FcDurSXanth$^{CF_3+\bullet}$** and the one-electron reduced form **FcDurSXanth$^{CF_3\bullet}$.**

References

1 L. A. Casper, M. Linseis, S. Demeshko, M. Azarkh, M. Drescher and R. F. Winter, *Chem. Eur. J.*, 2021, **27**, 10854-10868.
2 D. L. Reger, T. D. Wright, C. A. Little, J. J. Lamba and M. D. Smith, *Inorg. Chem.*, 2001, **40**, 3810–3814.
3 Y. Li, M. Josowicz and L. M. Tolbert, *J. Am. Chem. Soc.*, 2010, **132**, 10374–10382.
4 M. Brookhart, B. Grant and A. F. Volpe, *Organometallics*, 1992, **11**, 3920–3922.
5 magnettech by Freiberg Instruments, *Manual and documentation MiniScope MS5000 and MS5000X. EPR spectrometer with scientific grade performance*, Berlin, Germany, 6th edn., 2018.
6 L. A. Casper, L. Wursthorn, M. Geppert, P. Roser, M. Linseis, M. Drescher and R. F. Winter, *Organometallics*, 2020, **39**, 3275–3289.
7 S. Stoll and A. Schweiger, *J. Magn. Reson.*, 2006, **178**, 42–55.
8 S. S. Eaton and G. R. Eaton, *Bull. Magn. Reson.*, 1980, **1**, 130–138.
9 E. Bill, *MFit*, **2008**, Max-Planck Institute for Chemical Energy Conversion: Mülheim/Ruhr, Germany.
10 O. V. Dolomanov, L. J. Bourhis, R. J. Gildea, J. A. K. Howard and H. Puschmann, *J. Appl. Crystallogr.*, 2009, **42**, 339–341.
11 G. M. Sheldrick, *Acta Crystallogr. A*, 2015, **71**, 3–8.
12 G. M. Sheldrick, *Acta Crystallogr. C*, 2015, **71**, 3–8.
13 L. A. Casper, V. Ebel, M. Linseis and R. F. Winter, *Dalton Trans.*, 2021, **50**, 15336-15351.
14 M. J. Frisch, G. W. Trucks, H. B. Schlegel, G. E. Scuseria, M. A. Robb, J. R. Cheeseman, G. Scalmani, V. Barone, G. A. Petersson, H. Nakatsuji, X. Li, M. Caricato, A. V. Marenich, J. Bloino, B. G. Janesko, R. Gomperts, B. Mennucci, H. P. Hratchian, J. V. Ortiz, A. F. Izmaylov, J. L. Sonnenberg, Williams, F. Ding, F. Lipparini, F. Egidi, J. Goings, B. Peng, A. Petrone, T. Henderson, D. Ranasinghe, V. G. Zakrzewski, J. Gao, N. Rega, G. Zheng, W. Liang, M. Hada, M. Ehara, K. Toyota, R. Fukuda, J. Hasegawa, M. Ishida, T. Nakajima, Y. Honda, O. Kitao, H. Nakai, T. Vreven, K. Throssell, J. A. Montgomery Jr., J. E. Peralta, F. Ogliaro, M. J. Bearpark, J. J. Heyd, E. N. Brothers, K. N. Kudin, V. N. Staroverov, T. A. Keith, R. Kobayashi, J. Normand, K. Raghavachari, A. P. Rendell, J. C. Burant, S. S. Iyengar, J. Tomasi, M. Cossi, J. M. Millam, M. Klene, C. Adamo, R. Cammi, J. W. Ochterski, R. L. Martin, K. Morokuma, O. Farkas, J. B. Foresman and D. J. Fox, *Gaussian 16 Rev. C.01*, Wallingford, CA, USA, 2016.
15 M. Cossi, N. Rega, G. Scalmani and V. Barone, *J. Comput. Chem.*, 2003, **24**, 669–681.
16 B. P. Pritchard, D. Altarawy, B. Didier, T. D. Gibson and T. L. Windus, *J. Chem. Inf. Mod.*, 2019, **59**, 4814–4820.
17 P. C. Hariharan and J. A. Pople, *Theoret. Chim. Acta*, 1973, **28**, 213–222.
18 J. P. Perdew, K. Burke and M. Ernzerhof, *Phys. Rev. Lett.*, 1996, **77**, 3865–3868.
19 C. Adamo and V. Barone, *J. Chem. Phys.*, 1999, **110**, 6158–6170.
20 N. M. O'Boyle, A. L. Tenderholt and K. M. Langner, *J. Comput. Chem.*, 2008, **29**, 839–845.
21 M. D. Hanwell, D. E. Curtis, D. C. Lonie, T. Vandermeersch, E. Zurek and G. R. Hutchison, *J. Chem. Inf.*, 2012, **4**, 1–17.
22 O. Tange, *The USENIX Magazine*, 2011, **36**, 42.
23 S. Oßwald, Dissertation, University of Konstanz, 2019.
24 *Matlab*, TheMathWorks Inc.